

Kinetics of Excited-State Ti(a^5F) Depletion by NO, O₂, N₂O, and N₂

D. E. Clemmer, K. Honma,* and I. Koyano

Department of Material Science, Himeji Institute of Technology, 1479-1 Kanaji, Kamigori, Hyogo 678-12, Japan

Received: June 15, 1993; In Final Form: August 16, 1993*

The kinetics of depletion of ground-state Ti(a^3F) and excited-state Ti(a^5F) upon interactions with NO, O₂, N₂O, and N₂ are studied in a fast-flow reactor at a He pressure of 0.70 Torr. The technique is analogous to one introduced previously (*J. Phys. Chem.* 1989, 93, 1576) to study reaction of Ti(a^3F) with NO, O₂, and N₂O and uses a direct current discharge source to produce Ti atoms and laser-induced fluorescence detection. Our results confirm that Ti(a^3F) depletion by NO, O₂, and N₂O is inefficient and give 300 K effective bimolecular rate constants of $(7.3 \pm 0.8) \times 10^{-12}$, $(1.6 \pm 0.2) \times 10^{-12}$, and $(0.7 \pm 0.2) \times 10^{-12}$ cm³ s⁻¹, respectively, in agreement with previous work. In contrast to the Ti(a^3F) system, depletion of excited-state Ti(a^5F) upon interaction with NO, O₂, and N₂O is very efficient, and our measured effective bimolecular rate constants are $(146 \pm 17) \times 10^{-12}$, $(135 \pm 29) \times 10^{-12}$, and $\geq 190 \times 10^{-12}$ cm³ s⁻¹, respectively. We also report the effective bimolecular rate constant for quenching of Ti(a^5F) by N₂ at 300 K to be $(6.5 \pm 2.2) \times 10^{-12}$ cm³ s⁻¹. Reactive differences of Ti(a^3F) and Ti(a^5F) with these gases are discussed, and the implications of the present results on previously proposed mechanisms for oxidation of Ti by NO, O₂, and N₂O are considered.

Introduction

The kinetics associated with formation of transition metal oxides from the reactions of metal atoms with small molecules are important for understanding the chemistry that occurs during corrosion and in the atmosphere.¹ For this reason, a rather large data base has evolved for the kinetics of reactions of ionic transition metal atoms with small oxygen-containing molecules.^{2–14} Recently, the oxidation kinetics of neutral transition metal atoms have also received considerable attention.^{15–27}

One property of transition metal atoms that complicates kinetic measurements is the high density of low-lying electronic states that results from the near degeneracy of the ns and $(n-1)d$ (where n is the principal quantum number) orbitals. The reaction efficiencies of metal cations with many small molecules show a drastic dependence on the electronic state of the ion, and a detailed understanding of the role that the metal plays in these systems can only be assessed if its initial electronic state is well characterized.³ It seems likely that similar characterizations of the electronic states of neutral metal atoms will be necessary to fully understand their reactivities.

In this paper, we report the first measurements of the 300 K effective reaction rate constants for depletion of excited-state Ti(a^5F) from interactions with NO, O₂, and N₂O by using a flow-tube laser-induced fluorescence (LIF) technique introduced by Ritter and Weisshaar (RW).¹⁵ We have undertaken this work with three goals in mind. First, the results will extend the available kinetic data base for the reactions of neutral transition metal atoms with small oxidant molecules. Second, we will compare results for the reaction of Ti(a^5F) (having a valence electron configuration of $4s^13d^3$) with existing results for the reaction of ground-state Ti(a^3F) ($4s^23d^2$) to better understand the roles that different electronic states of the metal atom play in these systems. Finally, we will compare our results for the reaction of ground-state Ti(a^3F) with OX to those obtained previously in order to check the accuracy of the published data.

In their first study, which introduced the flow-tube LIF technique,¹⁵ RW measured bimolecular rate constants for reaction of ground-state Ti(a^3F) with NO, O₂, and N₂O via reaction 1.



The primary result was that oxidation is inefficient even though the overall energetics of these systems are favorable (Table I). RW rationalized this result by considering orbital correlation concepts. These ideas suggest the potential energy surfaces for reaction of Ti(a^3F) (having a valence electron configuration of $4s^23d^2$) are repulsive and TiO formation occurs over a barrier resulting from an avoided intersection of the Ti(a^3F) surface with a chemically attractive surface evolving from a Ti state having a $4s^13d^3$ configuration.¹⁵ For the reactions of Sc, Ti, and V with a given OX, this model predicts that rate constants should increase as $k(\text{Sc}) < k(\text{Ti}) < k(\text{V})$ since the energy differences of the $4s^23d^{n-2}$ (where n is the number of valence electrons) ground state and $4s^13d^{n-1}$ first excited state are 1.43, 0.81, and 0.26 eV,²⁹ respectively. However, the measured rate constants for a given OX are remarkably similar for all three metals, and the actual ordering is $k(\text{Ti}) < k(\text{V}) < k(\text{Sc})$.¹⁶

To explain their results for all three metal systems, RW invoked an electron-transfer mechanism similar to the well-known "harpoon" mechanism.^{16,21,30,31} In this mechanism, the potential surface for interaction of neutral $\text{M} + \text{OX}$ crosses an attractive $\text{M}^+ + \text{OX}^-$ ion-pair surface, and an electron may be transferred. TiO is then formed by O⁻ abstraction by Ti⁺. In this mechanism, variations in the kinetic data can be ascribed to differences in the metal ionization energies and the electron affinities of OX. This provides a qualitative explanation for the reaction efficiency of the three metal systems with a given OX. However, the mechanism predicts that for a given metal the rate constants should increase as $k(\text{N}_2\text{O}) < k(\text{NO}) < k(\text{O}_2)$, which is not observed experimentally.

Clearly, considerable progress in understanding the reactivity of ground-state metal atoms with OX has been made. However, little is known about the interaction of excited-state reaction surfaces in these systems. Debois and Gole (DG) have used chemiluminescence techniques to provide the only kinetic information regarding the reactivity of excited-state Ti with O₂ and N₂O.²¹ DG conclude that, for the reaction with O₂, C³Δ-X³Δ chemiluminescence of TiO* is overwhelmingly due to reaction of excited-state Ti atoms (likely a^5F atoms). However, in the N₂O reaction, chemiluminescence results from reaction of Ti(a^3F). While useful in understanding the electronic constraints associated with formation of excited TiO* states, these results do not give

* Abstract published in *Advance ACS Abstracts*, October 1, 1993.

TABLE I: Effective Bimolecular Rate Constants for Reactions of Ti(a^3F) and Ti(a^5F) with NO, O₂, N₂O, and N₂ at 300 K

reactants	$\Delta H_f^\circ_{298}$, ^a kcal/mol	k , 10 ⁻¹² cm ³ s ⁻¹ ^b (0.8 Torr He)	k , 10 ⁻¹² cm ³ s ⁻¹ ^b (0.4 Torr He)	k , 10 ⁻¹² cm ³ s ⁻¹ ^c (0.7 Torr He)	k_{HS}/k_{exp} ^d	E_{max} , ^e kcal/mol
Ti(a^3F_2) + NO	-7.5 ± 2.5	7.8 ± 0.2	9.5 ± 1.0	7.3 ± 0.8	35	2.1
Ti(a^3F_2) + O ₂	-39.3 ± 2.3	1.5 ± 0.2	1.9 ± 0.2	1.6 ± 0.2	155	3.0
Ti(a^3F_2) + N ₂ O	-118.5 ± 2.3	0.40 ± 0.05	0.44 ± 0.04	0.7 ± 0.2	370	3.5
Ti(a^3F_2) + N ₂	112 ± 8			NR ^f		
Ti(a^5F_1) + NO	-26.2 ± 2.5			146 ± 17	2	0.3
Ti(a^5F_1) + O ₂	-58.0 ± 2.3			135 ± 29	2	0.4
Ti(a^5F_1) + N ₂ O	-137.2 ± 2.3			≥190	1	<0.2
Ti(a^5F_1) + N ₂	93 ± 8			6.5 ± 2.2	45	

^a Values of $\Delta H_f^\circ_{298}$ are derived from $D^\circ_{298}(OX) - D^\circ_{298}(MO)$ and the data given in Table II. $D^\circ_{298}(TiO) = 158$ kcal/mol is from Pedley, J. B.; Marshall, E. M. *J. Phys. Chem. Ref. Data* 1983, 12, 967. The OX and N₂ bond energies are derived from data given in ref 46. $D^\circ_{298}(TiN) = 114 \pm 8$ kcal/mol as given in ref 47. ^b Ref 16. ^c This work. ^d Calculated by comparison of our experimental k_S to k_{HS} (see ref 44). ^e Values of E_{max} are estimated from the Arrhenius equation. $E_{max} = -RT \ln(k_{300}/k_{HS})$. ^f No reaction was observed. This implies that $k \leq 5 \times 10^{-14}$ cm³ s⁻¹ as discussed in the text.

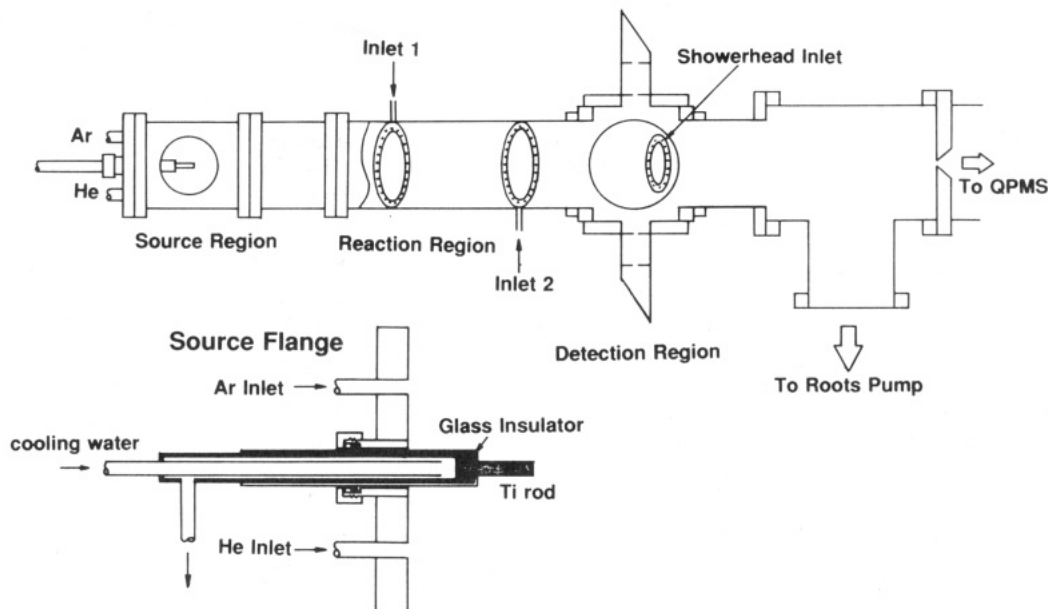


Figure 1. Schematic diagram of the flow-tube LIF apparatus. The apparatus is also equipped with a quadrupole mass spectrometer that was not used in these experiments.

information about the overall reactivities of Ti(a^3F) and Ti(a^5F) with OX since ground-state TiO($X^3\Delta$) could be formed and no chemiluminescence would be observed. Thus, our experiments should provide more direct information about the overall reactivities of these states.

Experimental Section

General. A schematic diagram of the flow-tube LIF apparatus used in these experiments is shown in Figure 1. The basic experiment is simple in concept. Metal atoms are created in a flow tube and are allowed to react for a well-defined period of time (at 300 K) with a reagent gas of known concentration. Then, LIF is used to detect the intensity of unreacted metal atoms in a specific state by probing a known atomic transition.

The flow tube shown in Figure 1 consists of three tubular stainless steel sections having an i.d. of 4.5 cm. End flanges sealed by o-rings on each tube allow the sections to be interchanged or eliminated to obtain flow tube lengths of 45, 35, 25, and 15 cm. In this work, only the 45-cm length is used. In this configuration, two reagent ring inlets 24 and 34 cm from the end of the flow tube are available. The ring inlets are made of 1/8-in. Cu tubing and fit snugly along the inside wall of the flow tube. The inside surface of each inlet contains ~20 pinholes such that reagent gas is introduced perpendicularly to the flow direction and uniformly toward the flow tube center from all directions. One shower head inlet where gas is introduced against the He flow is located 1 cm behind the LIF detection region (Figure 1).

The He buffer gas is introduced upstream from the reagent inlet ports at the end of the flow tube. He and reagent gas flows are regulated by needle valves and monitored by flow meters (KOFLOC Model 3710). The gases are pumped from the instrument by a Roots blower (Figure 1). To obtain a pressure of 0.70 Torr, the He flow rate was typically 4700–5000 standard (STP) cm³/min (sccm). The bulk average velocity of He under these conditions is calculated to be ~5500 cm/s. During a single experiment (which involved taking 5–30 data points and required ~30–90 min), the total flow tube pressure and He flow rate were stable to within 0.02 Torr and 50 sccm, respectively. A small amount of Ar was typically added in order to stabilize the discharge. The Ar concentration was always less than 5% of the He pressure and usually less than 2%. He(99.9999%), Ar(99.9999%), NO(99.9%), O₂(99.999%), N₂O(99.999%), and N₂(99.9999%) were obtained from NIHON SANSO and used without further purification. The total pressure in the flow tube was measured by a capacitance manometer (MKS Baratron, Type 122A).

Metal Atom Source. Figure 1 also shows a detailed schematic diagram of the flowing afterglow metal atom source used to produce Ti(a^3F) and Ti(a^5F) atoms for these experiments. Table II lists the low-lying electronic states, configurations, and energies of Ti. Because the transitions between the low-lying excited states are "spin" and parity forbidden, the lifetime is expected to be on the order of seconds.^{32,33} Our source is similar to two that have been discussed previously.^{34,35} A flow of ~95–99% He and 1–5% Ar is passed over a 5-cm-long, 0.5-cm-diameter Ti rod (Nilaco,

TABLE II: Configurations and Energies of the Low-Lying States of Titanium^a

configuration	term	<i>J</i>	energy, cm ⁻¹
3d ² 4s ²	a ³ F	2	0.000
		3	170.132
		4	386.874
3d ³ 4s ¹	a ⁵ F	1	6556.828
		2	6598.749
		3	6661.003
		4	6742.757
		5	6842.964
3d ² 4s ²	a ¹ D	2	7255.369
3d ² 4s ²	a ³ P	0	8436.618
		1	8492.421
3d ³ 4s ¹	b ³ F	2	8602.340
		2	11531.760
		3	11639.804
		4	11776.806

^a Data are taken from ref 29.

99.5%) that is biased at between -2.0 to -3.5 keV with respect to the flow tube. Ar⁺ and He⁺ created in the discharge are accelerated toward the Ti cathode, and Ti atoms are sputtered off. Ti atoms are swept downstream in the buffer gas flow and undergo $\sim 2 \times 10^4$ collisions with He and ~ 500 collisions with Ar before reaching the first reagent inlet port.

The Ti rod is threaded on one end and screwed directly into the glass-covered cathode support. This lessens arching along the edges of the Ti and cathode support connection and leads to a stable discharge surface. The glass covering electrically insulates the metal cathode from the flow tube body and prevents impurities (from sputtering of the cathode support) from complicating the flow tube system. A 100-k Ω electrical ballast is used to stabilize the discharge current. Under typical flow conditions, a 2.5-keV discharge voltage gives a current of 7–15 mA with respect to ground. A water cooling system is used to cool the cathode (Figure 1). Although this source produces mainly Ti(a³F) atoms, Ti(a⁵F) atoms are easily produced in quantities necessary for these experiments. RW mentioned that they can easily detect these species as well as Ti(a¹D) and Ti(a³P) by using a laser vaporization source.¹⁵

Flow Characteristics and Reaction Region Temperature. The flow tube used in this study has a smaller i.d. compared with that of RW. We used slightly lower He pressure and slower flow rate. As the result of these values, the Reynolds number of our flow tube is about half of that of the flow tube of RW, and this gives 8 cm of the distance necessary for He to develop its characteristic parabolic velocity profile. Therefore, we believe that the flow in our tube is fully developed at the first inlet of reactant located 24 cm from the end of the flow tube.

The temperature of the reaction region was measured by a Chromel–Alumel thermocouple gauge referenced to 0 °C by using an ice bath. At a total pressure of 0.70 Torr and a discharge voltage of 2.5 keV, the temperature at the beginning of the reaction region in the center of the flow tube is 23 °C (essentially room temperature). The temperature is 19 °C at the edge of the flow tube, and similar radial temperature distribution was seen by RW. Upon immediate removal of the cathode source from the instrument after operating at 2.5 keV for more than 3 h, the Ti cathode rod is cool to the touch. Since room temperature could have fluctuated by several degrees from day to day during the several months over which these experiments were carried out, our reported thermochemistry is given at $T = 300$ K rather than 296 K.

Reaction Region Time. The flight time of Ti atoms through the reaction region was measured by using pulsed laser vaporization to generate Ti* and monitoring the spectrally unresolved fluorescence signal of these species 40 cm downstream at the LIF viewing region as a function of the time after the laser pulse.³⁶ Figure 2 shows the arrival time of the fluorescence signal at a

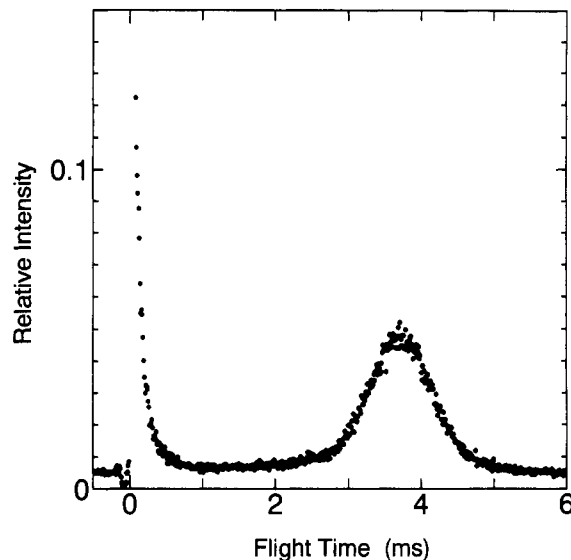


Figure 2. Arrival time distributions from source to detection region (40 cm) at 0.7 Torr He. The first narrow peak is due to the initial laser vaporization pulse, and the second broader peak is due to fluorescence of Ti*.

TABLE III: LIF Transitions Used To Probe Ti(a³F) and Ti(a⁵F)^a

species	transition	energy, cm ⁻¹	wavelength, nm
Ti(a ³ F)	y ³ F ₂ –a ³ F ₂	25 107.417	398.29
	y ³ F ₃ –a ³ F ₃	25 057.085	399.09
	y ³ F ₄ –a ³ F ₄	25 001.460	399.98
Ti(a ⁵ F)	x ⁵ D ₀ –a ⁵ F ₁	23 272.269	429.70
	x ³ D ₁ –a ⁵ F ₂	23 256.499	429.99
	x ³ D ₂ –a ⁵ F ₃	23 246.270	430.18
	x ³ D ₃ –a ⁵ F ₄	23 243.428	430.23
	x ³ D ₄ –a ⁵ F ₅	23 217.364	430.71

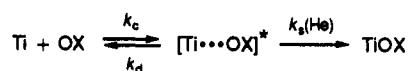
^a Energies and wavelengths are derived from data in ref 29.

flow tube pressure of 0.70 Torr (He only). Indistinguishable results were obtained when 1–5% Ar was added to the flow. The first narrow peak is scattered laser light, and the second broader peak is due to Ti* fluorescence. The maximum in the signal appears 3.8×10^{-3} s after the laser pulse and has a fwhm of 1.1×10^{-3} seconds.

RW have shown that Ti(a³F), Ti*(a³P), Ti*(a⁴F), and TiO-(X³Δ)³⁷ have the same mean velocities for flow tube lengths from 30 to 140 cm.¹⁵ To determine the mean Ti reaction time (for our 21-cm reaction zone), we assume that the mean velocity of all species contributing to the fluorescence signal is constant over the 40-cm distance. This assumption is reasonable since the fwhm of the data shown in Figure 2 for a flow length of 40 cm is about 3 times less than the fwhm of the flight time data for arrival of only the Ti(a³F) state shown in RW's paper for a flow length of 117.5 cm.¹⁵ (If the many species that radiate in our system had different velocities then we would expect a much broader peak.) Thus, $\langle v_{Ti} \rangle$ at 0.70 Torr is $\sim 10\,500$ cm/s, and the mean reaction time for the 21-cm reaction zone is 2.0×10^{-3} s. Sticking of metal atoms to the flow tube surface is expected to be efficient.^{15,38} Thus, the observation that $\langle v_{Ti} \rangle$ is greater than $\langle v_{He} \rangle$ indicates that the Ti density is largest in the center of the flow tube where the He axial velocity is largest.

LIF Detection. Ti atom number densities in specific states are measured by using unsaturated LIF as verified by linearity in the LIF signal with laser power. The transitions and energies used for detecting the three *J* levels of Ti(a³F) and the five *J* levels of Ti(a⁵F) are given in Table III. A Nd:YAG (10 Hz, 10-ns fwhm) laser is used to pump a tunable titanium sapphire laser capable of generating intense light from ~ 740 –900 nm. To obtain the ~ 400 - and ~ 430 -nm light used in these studies, ~ 800 - and ~ 860 -nm light was frequency doubled using a KDP crystal. Over

SCHEME I



several hours, the intensity of the laser is stable to within $\pm 20\%$. Figure 1 shows that the laser beam enters and exits the detection region of the instrument through Suprasil windows at the Brewster angle. An entrance system 31 cm long and containing four baffles is used to minimize the scattered light. Spectrally unresolved fluorescence is collected by a lens system and focused through a 2.0-mm slit into a photomultiplier tube (PMT) (HAMAMATSU Photonics R-928). The PMT current is amplified by a wide-band preamplifier (NF Electronics, Model BX-31), and the amplified voltage pulse is integrated by a boxcar integrator (SRS, Model SR-250). The unresolved LIF signal is viewed on an oscilloscope, and the time-integrated intensity is stored via computer. Current due to scattered light is insignificant in the Ti(a³F) experiments but comprises $\sim 10\text{--}50\%$ of the signal in the Ti(a⁵F) experiments.

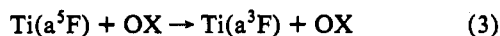
Before collecting kinetic data, the laser was scanned over a wide wavelength region ($\sim 10\text{--}20$ nm) in order to determine the experimental position of each transition and assign each line. The atomic transitions are sufficiently narrow that when the laser is tuned to a transition, small drifts in the laser frequency lead to large fluctuations in the LIF signal. To avoid this problem in determining the LIF intensity as a function of OX flow, the laser was tuned over each transition slowly (a range of 0.01 nm at 0.001 nm/s) for every OX flow rate so that the maximum signal was never missed. This also allows us to distinguish the scattered light from the Ti LIF signal since the scattered light becomes the baseline signal.

Quenching of the y³F and x⁵D Excitation States. Collisions with He, Ar, and the oxidant gas could quench or react with the y³F and x⁵D excitation states that are used to detect Ti in this study and decrease the observed LIF signal. We have tested this for the y³F–a³F transition by introducing the reagent gas at the shower head inlet near the LIF viewing region. Koyano and co-workers have utilized this experimental configuration of the present apparatus to study collisional relaxation of vibrationally and electronically excited states of CO⁺.^{39–41} Below 100 sccm, no decrease in the LIF intensity for any of the oxidant gases is observed. Above this flow rate, the signal decreases slowly. Therefore, we conclude that quenching collisions in the LIF detection region of our instrument are insignificant below 100 sccm and larger flow rates are not used.

Kinetics. The time-integrated rate expression for a simple bimolecular process such as reaction 1 is given by eq 2.

$$\ln[\text{Ti}(n_{\text{OX}})/\text{Ti}_0] = -k_{\text{rxn}} t_{\text{rxn}} n_{\text{OX}} \quad (2)$$

Here, Ti(*n*_{OX}) is the time-integrated metal atom concentration, Ti₀ is the titanium intensity when no OX gas is present, *k*_{rxn} is the bimolecular rate constant, *t*_{rxn} is the mean reaction time, and *n*_{OX} is the oxidant number density. Although it is likely that the main process for depletion of Ti(a³F) by NO, O₂, and N₂O is via reaction 1, as discussed below, the kinetic expression for the Ti-(a⁵F) system is complicated since quenching via process 3, might also deplete the Ti signal.



In this case, the time-integrated rate expression is given by eq 4,

$$\ln[\text{Ti}(n_{\text{OX}})/\text{Ti}_0] = -(k_{\text{rxn}} + k_q) t_{\text{rxn}} n_{\text{OX}} \quad (4)$$

where *k*_q is the quenching rate constant for process 3.

The only other process that can deplete the Ti(a³F) and Ti-(a⁵F) signals is termolecular association via the mechanism given in Scheme I. Here, [Ti⋯OX]^{*} formed at the total collision rate constant (*k*_c) may be stabilized by collisions with He (at *k*_s) or

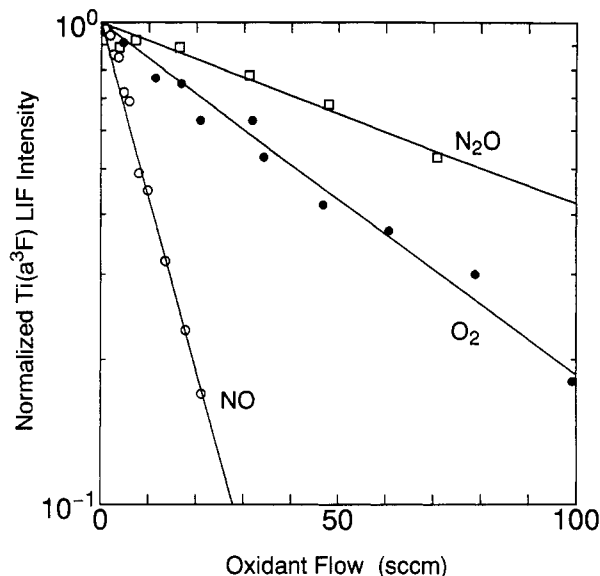


Figure 3. Semilogarithmic plots of the Ti(*n*_{OX})/Ti₀ LIF intensities for Ti(a³F) vs flow of NO, O₂, and N₂O. The solid lines are optimized least-squares fits of eq 2 to the data.

unimolecularly dissociate back to reactants (at *k*_d). Scheme I gives the pressure-dependent rate constant (*k*_a) for TiOX formation given by eq 5,

$$k_a(P) = k_s k_c P \beta / (k_d + k_s P \beta) \quad (5)$$

where $\beta = 1/k_B T$, *k*_B is Boltzmann's constant, and *P* and *T* are the He gas pressure and the He gas pressure and temperature, respectively. Clear evidence of Scheme I may be seen at low *P*, where eq 5 simplifies to *k*_a(*P*) = *k*_s*k*_c*P* β /*k*_d and the measured rate constant depends linearly on *P*. However, no *P* dependence does not rule out Scheme I since at high *P* eq 5 simplifies to *k*_a = *k*_c.

RW discussed that an upper limit for Scheme I depletion of Ti(a³F) can be obtained from the termolecular association reactions of M⁺ (M = Mg, Ca, and Ba) with O₂, CO, and CO₂ using He as a third body.⁴² The overall kinetics for these systems are slow ($\sim 3 \times 10^{-30}$ cm⁶ s⁻¹) but are good upper limits to contributions in the present system because the ion–molecule forces should be much stronger and longer range than the weak interactions in the neutral systems. This comparison shows that the maximum depletion by Scheme I (at 0.7 Torr He) is $\sim 0.07 \times 10^{-12}$ cm³ s⁻¹. Except for the kinetics for depletion of Ti(a³F) by N₂O (Table I), this small contribution to the measured depletion rates is negligible in the present systems.

Because the depletion signal that we measure could be affected by reactions 1 and 3 (and to a small extent Scheme I), our reported rate constants are referred to as *effective* values rather than absolute values. Effective state-specific 300 K bimolecular rate constants are derived by fitting semilogarithmic plots of the data using a least-squares routine. We report 2 σ uncertainties for the precision of the fits to multiple data sets. The absolute accuracies of the rate constants are estimated to be $\pm 30\%$ for Ti(a³F) and $\pm 40\%$ for Ti(a⁵F) and are limited mainly by fluctuations in laser power and source atom production. Other smaller contributions to our absolute uncertainty are from the measurement of *t*_{RXN}, incomplete mixing of the reagent gases, and the accuracy of the flow rate and pressure measurements. We estimate the absolute sensitivity of our instrument to be $\sim 5 \times 10^{-14}$ cm³ s⁻¹ based on our ability to easily observe a 5% decrease in our signal at a reagent gas flow rate of 100 sccm.

Results

Ti(a³F) + OX. Figure 3 shows semilogarithmic plots of the Ti(*n*_{OX})/Ti₀ signals for Ti(a³F) for flow rates of NO, O₂, and

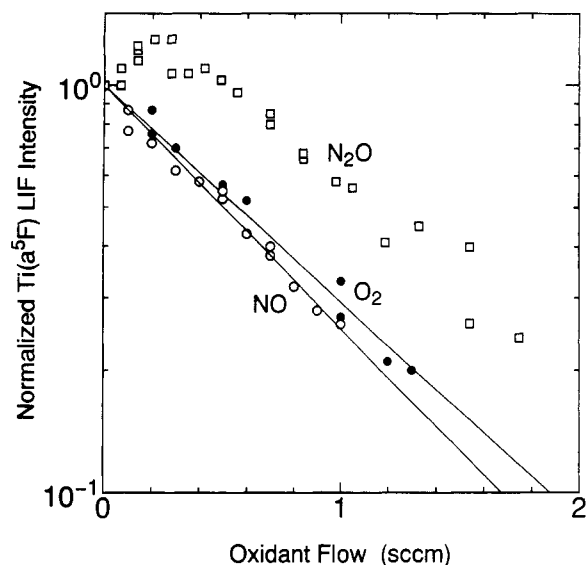


Figure 4. Semilogarithmic plots of the $Ti(n_{OX})/Ti_0$ LIF intensities for $Ti(a^5F)$ vs flow of NO, O_2 , and N_2O . The solid lines are optimized least-squares fits of eq 2 to the data.

N_2O from 0–100 sccm at a He pressure of 0.70 Torr. The plots for all three J levels of $Ti(a^3F_j)$ are indistinguishable within the uncertainty of the data, and the depletion rates increase as $N_2O < O_2 < NO$.

The effective bimolecular rate constants derived from these data for the reaction of $Ti(a^3F)$ with NO, O_2 , and N_2O are (7.3 ± 0.8) , (1.6 ± 0.2) , and $(0.7 \pm 0.2) \times 10^{-12} \text{ cm}^3 \text{ s}^{-1}$, respectively (Table I). Within the precision of our measurements, the NO and O_2 results are in excellent agreement with RW's best data taken at 0.8 Torr He. Our rate constant for the $Ti(a^3F) + N_2O$ system is slightly larger than RW's values at 0.8 and 0.4 Torr (Table I). However, within the combined absolute uncertainty of both experiments, the data are in agreement. The agreement of our results with those of RW shows that there are no obvious problems concerning the characterization of instrumental parameters such as t_{RXN} and the temperature of the reaction region in our instrument.

$Ti(a^5F) + OX$. Figure 4 shows semilogarithmic plots of the $Ti(n_{OX})/Ti_0$ signals for $Ti(a^5F)$ as a function of the flow rates of NO, O_2 , and N_2O (over a 0–2 sccm range) at a He pressure of 0.70 Torr. As observed for the reaction of $Ti(a^3F)$, no differences in the reactivity of the five J levels of $Ti(a^5F_j)$ are observed. The most striking difference between these data and the $Ti(a^3F)$ data is that $Ti(a^5F)$ is depleted much more rapidly by all three gases. It is also clear that the kinetics associated with depletion of $Ti(a^5F)$ by NO and O_2 are nearly identical, while for $Ti(a^3F)$, NO reacts ~ 5 times more efficiently than O_2 . The effective bimolecular rate constants derived for the depletion of $Ti(a^5F)$ from interactions with NO and O_2 are (146 ± 17) and $(135 \pm 29) \times 10^{-12} \text{ cm}^3 \text{ s}^{-1}$ and are listed in Table I.

The observation of no systematic dependence of depletion of different J levels of $Ti(a^3F_j)$ is consistent with the results of RW.¹⁵ RW have also found no variations in the rate constants for reaction of the different J levels of ground-state $Sc(a^2D_j)$ and $V(a^4F_j)$ with these oxidants.¹⁶ These results indicate that either the rate constants for individual J levels for both states are the same within the experimental sensitivity or the reaction rate is much slower than interconversion of J levels from collisions with He, Ar, or OX. Our data for depletion of excited-state $Ti(a^5F_j)$ also show no J dependence in these systems and indicate either that the rates for different J levels are the same or that the reaction rate is much slower than the rates for interconversion. However, in the latter case collisional interconversion must come from interactions with He or Ar since OX collisions result in $Ti(a^5F)$ depletion with near unit efficiency (Table I).

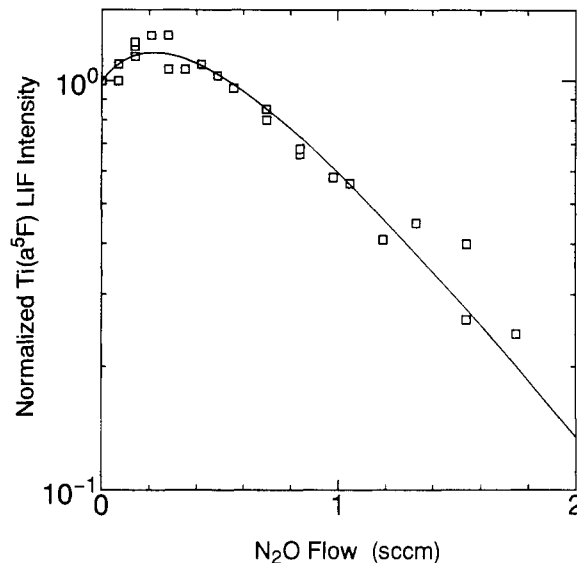
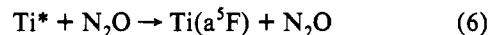


Figure 5. Semilogarithmic plot of the $Ti(n_{OX})/Ti_0$ LIF intensities for $Ti(a^5F)$ vs N_2O flow. The solid line is the optimized least-squares fit to the two-exponential profile given by eq 7.

The depletion profile for the interaction of $Ti(a^5F)$ with N_2O is unique in that at flow rates below 0.4 sccm the intensity of the $Ti(a^5F)$ signal increases, while above this pressure the signal decreases rapidly. This behavior indicates that there are species present in the flow that upon collisions with N_2O form $Ti(a^5F)$. Presumably these are high-lying excited Ti^* states that are quenched via process 6.⁴³



Because the Ti source conditions in the N_2O system are identical to the NO and O_2 systems, the latter gases must either react with these higher lying states to form TiO or be inefficient at quenching the excited state to produce $Ti(a^5F)$.

Determination of the effective rate constant for depletion of $Ti(a^5F)$ from interactions with N_2O is complex because the initial concentrations of Ti^* states and the quenching rate constants are unknown. To proceed further in understanding the N_2O system, we have modeled the data with the kinetic expression given by eq 7

$$\begin{aligned} [Ti(n_{OX})/Ti_0] = & \\ & \{1 + k_6/(k_6 - k_1)\} [Ti^*/Ti_0] \exp(-k_1 t_{rxn} n_{OX}) - \\ & k_6/(k_6 - k_1) [Ti^*/Ti_0] \exp(-k_6 t_{rxn} n_{OX}) \quad (7) \end{aligned}$$

for a $[Ti(n_{OX})/Ti_0]$ signal that is depleted by reaction 1 (at k_1) and enhanced by process 6 (at k_6). $[Ti^*/Ti_0]$ is the ratio of initial Ti^* and $Ti(a^5F)$ populations. There are three unknowns in eq 7; k_1 , k_6 , and the $[Ti^*/Ti_0]$ ratio. We assume that k_6 proceeds at the total collision limit given by the hard-sphere (HS) rate constant⁴⁴ ($256 \times 10^{12} \text{ cm}^3 \text{ s}^{-1}$) and allow k_1 and $[Ti^*/Ti_0]$ to optimize using a least-squares routine. The resulting fit is shown in Figure 5 and clearly accounts for the two-exponential behavior displayed by the data. The optimum parameters, $[Ti^*/Ti_0] = 1.5$ and $k_1 = 190 \times 10^{-12} \text{ cm}^3 \text{ s}^{-1}$, suggest that the initial Ti^* concentration is ~ 1.5 times greater than that of $Ti(a^5F)$ and that depletion of $Ti(a^5F)$ by N_2O occurs rapidly as observed in the NO and O_2 systems. If k_6 is less than the HS collision limit, then values of k_1 and $[Ti^*/Ti_0]$ must increase to fit the data. Therefore, the value of $k_1 = 190 \times 10^{-12} \text{ cm}^3 \text{ s}^{-1}$ should be a valid lower limit for depletion of $Ti(a^5F)$ by N_2O .⁴⁵

The similar rise and decay profile may be expected for the depletion profile for the interaction of $Ti(a^3F)$ with OX, since a part of the depletion of $Ti(a^5F)$ could be quenching process to form $Ti(a^3F)$. However, no depletion profile of $Ti(a^3F)$ shows a rise at low flow rate region. This is reasonable since the relative

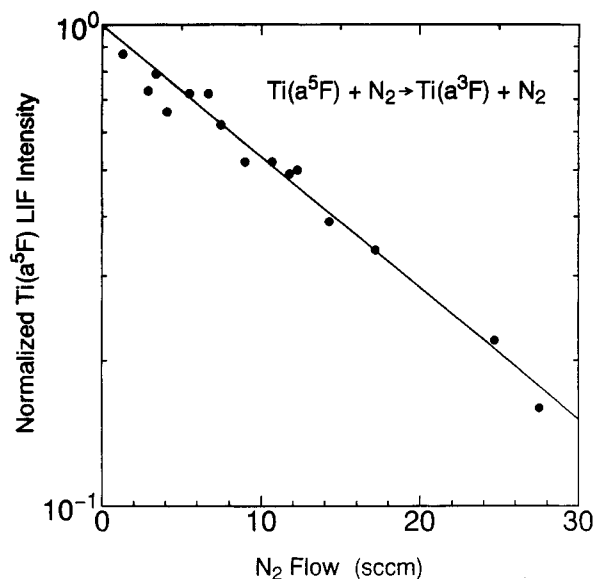


Figure 6. Semilogarithmic plot of the $Ti(n_{OX})/Ti_0$ LIF intensities for $Ti(a^5F)$ vs N_2 flow. The solid line is the optimized least-squares fit of eq 2 to the data.

concentration of $Ti(a^5F)$ is much smaller than that of $Ti(a^3F)$ ⁴⁶ and the quenching rate of $Ti(a^5F)$ is much faster than the depletion of $Ti(a^3F)$.

$Ti(a^3F)$ and $Ti(a^5F) + N_2$. Figure 6 shows the semilogarithmic plot of the $Ti(n_{OX})/Ti_0$ signal for depletion of $Ti(a^5F)$ as a function of the N_2 flow rate. All J states behave identically within the sensitivity of the experiment. Formation of TiN from the reaction of $Ti + N_2$ is endothermic by 112 ± 8 and 93 ± 8 kcal/mol for $Ti(a^3F)$ and $Ti(a^5F)$, respectively,^{47,48} and so it is not a thermodynamically feasible pathway. Therefore, the decay shown in Figure 6 must be due to quenching of $Ti(a^5F)$ to form $Ti(a^3F)$. Analysis of these data gives the effective quenching rate constant $k_q = (6.5 \pm 2.2) \times 10^{-12} \text{ cm}^3 \text{ s}^{-1}$. No depletion of ground-state $Ti(a^3F)$ for any J level is observed upon interaction with N_2 at flow rates up to 100 sccm.

Discussion

Collisional Quenching of $Ti(a^5F)$. Because the $Ti(a^5F)$ LIF signal could be depleted by forming $Ti(a^3F)$ (reaction 3) as well as TiO (reaction 1), it is important to consider the efficiency and mechanism of the quenching process. The $Ti(a^5F) + N_2$ system is a good starting point, since no bimolecular chemical processes are thermodynamically feasible and depletion of $Ti(a^5F)$ due to Scheme I cannot account for the measured rate constant, $(6.5 \pm 2.2) \times 10^{-12} \text{ cm}^3 \text{ s}^{-1}$.

Probably the simplest means of understanding the quenching process is to consider the potential energy surfaces that evolve from the low-lying states of Ti as the reagents approach. Figure 7 shows a qualitative sketch of the potential energy surfaces associated with the interaction of the five lowest energy states— $Ti(a^3F)$, $Ti(a^5F)$, $Ti(a^1D)$, $Ti(a^3P)$, and $Ti(b^3F)$ —with $N_2(^1\Sigma_g^+)$. We expect that the attractive $Ti + N_2$ interactions are weak and have little effect on the quenching process. Therefore, simplified surfaces which consider only the repulsive interactions are drawn. The low-lying states of Ti have electron configurations of $4s^23d^2$ or $4s^13d^3$. Due to the large spacial extent of the closed $4s$ subshell, the surfaces evolving from the a^3F , a^1D , and a^3P states (having a valence configuration of $4s^23d^2$) are expected to be repulsive at longer $Ti + N_2$ reagent distances than those evolving from the a^5F and b^3F ($4s^13d^3$) states, where the $4s$ orbital is only singly occupied. As the Ti and N_2 reagent distance lessens, surfaces evolving from the a^3F and a^5F states cross. In the free Ti atom, the a^5F – a^3F transition is both spin and parity forbidden. Thus, the crossing involves a spin–orbit interaction that effectively moves

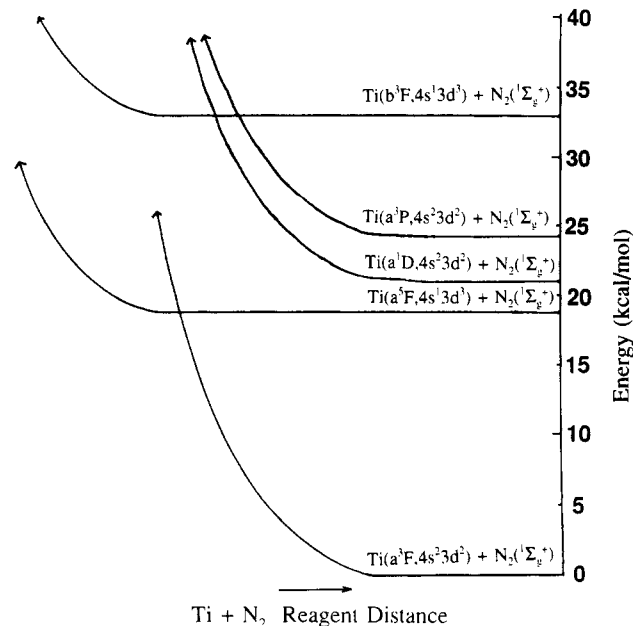


Figure 7. Qualitative potential energy surfaces showing the repulsive interactions of the five lowest electronic states of Ti with $N_2(^1\Sigma_g^+)$. The distance between reagents decreases from right to left in this figure.

one unpaired electron from a $3d$ orbital and places it into the $4s$ orbital. While we have little available information on this system, a comparison of k_q to the HS collision rate constant shows that $Ti(a^5F)$ is quenched on ~ 1 in 45 collisions with N_2 (Table I). Thus, the low probability of making this crossing during a collision with N_2 leads to a rate constant that is much less than the depletion rates measured for the $Ti(a^5F) + OX$ systems.

One feature of the $NO(^2\Pi)$ and $O_2(^3\Sigma_g^-)$ gases that may increase their ability to promote a quintet to triplet crossing is that they allow the overall quenching process, reaction 3, to conserve electronic spin. This is not the case for $N_2O(^1\Sigma^+)$. Thus, spin conservation cannot explain the increased depletion rate of all three oxidants.

An alternate explanation of the more efficient depletion of $Ti(a^5F)$ by all three oxidants compared with N_2 is that oxidation via reaction 1 occurs efficiently. Several other experimental results support this idea. First, TiO formed via reaction 1 has been directly detected for all three OX systems using LIF,¹⁵ and chemiluminescence of TiO^* for the $Ti + O_2$ and N_2O systems has been detected by us and other groups.^{21,25,49} Second, DG have shown that $C^3\Delta$ – $X^3\Delta$ chemiluminescence of TiO^* in the reaction of Ti with O_2 is overwhelmingly due to reaction of excited-state Ti , likely the $Ti(a^5F)$ state.²¹ As discussed below and previously,^{15,21} formation of TiO from reaction of Ti states having an electron configuration of $4s^13d^3$ (such as the a^5F state) should be more efficient than from reaction of $Ti(a^3F, 4s^23d^2)$. Finally, in our present results and in RW's study,¹⁵ no increase in the $Ti(a^3F)$ signal due to quenching or excited states was observed. While we expect that the population of excited states in our flow tube is small relative to the $Ti(a^3F)$ population, in RW's apparatus excited states comprise as much as 10% of the total population even 35–45 cm downstream from the source.¹⁵ The observation that their kinetic data shown no signs of quenching due to interactions with OX is consistent with a reaction 1 rate constant that is substantially larger than k_q for process 3. Assuming that values of k_q for the $Ti + OX$ systems are similar to $k_q = (6.5 \pm 2.2) \times 10^{-12} \text{ cm}^3 \text{ s}^{-1}$ measured for the $Ti(a^5F) + N_2$ system shows that quenching accounts for less than 5% of the signal decrease that we observe, well within the reported uncertainties (Table I).

One final point involving the surfaces shown in Figure 7 is that there are no obvious crossings of the surface evolving from the $Ti(a^5F)$ state and higher-lying surfaces. Clearly, these qualitative sketches are not easily extended to the N_2O system in order to

explain quenching of a higher-lying Ti^* species to form $Ti(a^5F)$. This suggests that quenching in the $Ti + N_2O$ system is more complex than the simple ideas put forth for the N_2 system. The observation that N_2O quenches Ti^* to form $Ti(a^5F)$, while NO and O_2 do not, suggests that the latter oxidants react with Ti^* to form TiO while N_2O is unreactive. The unreactive nature of N_2O with $Ti(a^3F)$ and metal cations has been attributed to an electronic constraint present in N_2O .^{9,15} In order to conserve spin, breaking the N_2-O bond involves diabatic dissociation of $N_2O(^1\Sigma^+)$ to form excited state $O(^1D)$ and $N_2(^1\Sigma_g^+)$. Presumably this electronic property of N_2O prevents it from reacting with Ti^* and allows it to act as a quenching gas.

Reaction Efficiencies and Activation Energies. In contrast to the large variations in the rate constants observed for the inefficient reactions of ground-state $Ti(a^3F)$ with NO , O_2 , and N_2O , depletion of $Ti(a^5F)$ by these gases is efficient in all three systems. Assuming that the a^5F rate constants are due primarily to reaction 1 shows that reaction of $Ti(a^5F)$ is more efficient than reaction of ground-state $Ti(a^3F)$ with the NO , O_2 , and N_2O oxidants by factors of ~ 20 , ~ 80 , and ~ 270 (Table I). For the O_2 system, this increase in reactivity is consistent with the observations of DG that $C^3\Delta-X^3\Delta$ chemiluminescence of TiO^* is overwhelmingly due to reaction of excited-state Ti , likely the $Ti(a^5F)$ state.²¹ In this system, formation of $TiO(C^3\Delta)$ is endothermic by 14 kcal/mol for reaction of $Ti(a^3F)$ and exothermic by 5 kcal/mol for reaction of $Ti(a^5F)$. Thus, one contributing factor to the increased reactivity for the O_2 system is that there are more available product channels for the reaction of $Ti(a^5F)$ than for $Ti(a^3F)$. This is also true for the NO system, since singlet states of TiO are accessible only for reaction of $Ti(a^5F)$. Given the large increase in reactivity observed for the reaction of $Ti(a^5F)$ with N_2O compared with $Ti(a^3F)$, it is interesting that DG did not observe changes in their chemiluminescence data due to $Ti(a^5F)$ reactions. This suggests that reaction of $Ti(a^5F) + N_2O$ produces mainly ground-state $TiO(X^3\Delta)$, which cannot be detected by chemiluminescence.

Assuming that these systems are governed by an Arrhenius behavior (i.e., $k(T) = Ae^{-E/kT}$), RW used HS rate constants to estimate upper limits for the A factor (A_{max}) and calculated upper limits for the activation energy (E_{max}) of 2.1, 3.1, and 3.9 kcal/mol for the $Ti(a^3F) + NO$, O_2 , and N_2O reactions, respectively.¹⁵ If we assume that reaction 1 is the dominant process for the decay observed, we can use our kinetic data to calculate E_{max} values of 0.3, 0.4, and <0.2 kcal/mol for the reactions of $Ti(a^5F)$ with NO , O_2 , and N_2O , respectively. Clearly, the large reaction barriers that were suggested as the explanation for the inefficiency of the ground-state $Ti(a^3F)$ reactions¹⁵ are not present in the reaction of excited-state $Ti(a^5F)$.

Reaction Mechanism. Two mechanisms have been proposed to explain the slow rates of O atom abstraction from reaction of $Ti(a^3F)$ with OX : a mechanism where the O atom is transferred directly to the neutral Ti atom and a mechanism that involves an electron-transfer (ET) process to form $Ti^+ + OX^-$ followed by O-atom transfer to Ti^+ . In the mechanism involving O atom abstraction by neutral Ti, RW proposed that a reaction barrier existed in the entrance channel of the $Ti(a^3F) + OX$ interaction. The rationale for this barrier was given in detail in their paper.¹⁵ Briefly, a qualitative orbital correlation argument was used to assert that barriers are expected along adiabatic surfaces where ground-state reactants and a specified set of product states do not correlate⁵⁰ to the same low-energy $Ti + O + X$ asymptote. Except for $TiO(d^1\Sigma^+, 8\sigma^2 3\pi^4 9\sigma^2)$ at an excitation energy of 0.7 eV,⁵¹ all of the low-lying TiO states have an electron configuration of $8\sigma^2 3\pi^4 9\sigma^1 1\delta^1$ (where the 9σ orbital is primarily $Ti(4s)$ in character)⁵² which can correlate to the $Ti(4s^1 3d^3)$ excited states but not to $Ti(a^3F, 4s^2 3d^2)$. Consequently, barriers arise when repulsive $Ti(a^3F, 4s^2 3d^2)$ surfaces, which must diabatically correlate to high-lying TiO states, cross attractive $Ti(4s^1 3d^3)$ surfaces

that can correlate to the low-lying TiO states. Our present results for reaction of excited-state $Ti(a^5F, 4s^1 3d^3)$ are consistent with the idea that there are no large barriers associated with the reaction of the $4s^1 3d^3$ configured states since the measured rate constants are much larger than the values measured for reaction of $Ti(a^3F, 4s^2 3d^2)$. Thus, O atom abstraction directly by neutral $Ti(a^5F)$ is a plausible mechanism.

As mentioned in the Introduction section, the mechanism involving O atom abstraction by a neutral metal atom incorrectly predicts that the rate constants for reaction of $Sc(a^2D)$, $Ti(a^3F)$, and $V(a^4F)$ should increase as $k(Sc) < k(Ti) < k(V)$ since the energy differences of the $4s^2 3d^{n-2}$ ground states and $4s^1 3d^{n-1}$ first excited states of these metals are 1.43, 0.81, and 0.26 eV, respectively. In order to qualitatively explain their rate constants for the reactions of $Sc(a^2D)$, $Ti(a^3F)$, and $V(a^4F)$ with NO , O_2 , and N_2O , RW invoked an ET mechanism similar to the well-known harpoon mechanism.¹⁶ The main idea of this mechanism is that a potential surface corresponding to the interaction of an $M^+ + OX^-$ ion pair crosses the surface for the interaction of the ground-state neutral reactants. At the crossing point, an electron jump can occur. Formation of TiO occurs by transfer of O^- from OX^- to Ti^+ .

An elegant feature of this mechanism is that the crossing point, R_x , of the $M^+ + OX^-$ ion-pair surface with any M or $M^+ + OX$ neutral surface can be calculated by eq 8,^{21,53}

$$R_x = e^2 / (IE(M) - EA(OX) - E_{el}(M)) \quad (8)$$

where e is the electron charge, $IE(M)$ is the ionization energy of the metal ($IE(Ti) = 6.820$ eV),²⁹ $EA(OX)$ is the electron affinity of OX ,⁵⁴ and $E_{el}(M)$ is the energy of the electronic state (Table II). Equation 8 makes the assumption that the neutral surface is flat, which is valid at long ranges because the neutral interactions are weak. For the $Ti(a^3F) + NO$, O_2 , and N_2O systems, eq 8 gives values of $R_x = 2.12$, 2.26, and 2.05 Å, respectively, and suggests that the electron transfer occurs at close range. Values of R_x can be converted to an upper limit for the ET rate constants (k_{ET}) by assuming that the crossing is made with unit efficiency and utilizing the relation $k_{ET} = \pi R_x^2 \langle v \rangle$ (where $\langle v \rangle$ is the mean relative velocity of the reactants). Values of k_{ET} for the $Ti(a^3F) + NO$, O_2 , and N_2O systems are 80×10^{-12} , 90×10^{-12} , and 70×10^{-12} $cm^3 s^{-1}$, respectively. These rate constants are much larger than the measured values given in Table I and do not follow the $k(N_2O) < k(O_2) < k(NO)$ ordering measured. However, when the scandium and vanadium metal systems are also considered, eq 8 does predict the ordering of the rate constants for reaction of ground-state $Sc(a^2D)$, $Ti(a^3F)$, and $V(a^4F)$ with a given OX : $k(Ti) < k(V) < k(Sc)$.

When applied to the reaction of $Ti(a^5F)$ with NO , O_2 , and N_2O , eq 8 predicts crossing distances, R_x , of 2.41, 2.59, and 2.32 Å and leads to values for the ET rate constants of 110×10^{-12} , 120×10^{-12} , and 90×10^{-12} $cm^3 s^{-1}$, respectively. For all three systems, the ET model qualitatively predicts the increase in the reactivity of the $Ti(a^5F)$ excited state, and for the NO and O_2 systems the calculated values are in close quantitative agreement with the measured rate constants (Table I). For the N_2O system, the value of $k_{ET} = 90 \times 10^{-12}$ $cm^3 s^{-1}$ is somewhat smaller than the lower limit of 190×10^{-12} $cm^3 s^{-1}$ measured for this system.⁵⁵

To test the ET mechanism further, we consider the reaction of excited-state $V(a^6D)$ with NO and O_2 . While $IE(V) = 6.74$ eV is similar to $IE(Ti) = 6.82$ eV, the electronic energy of $V(a^6D)$ is only 0.26 eV compared with $E_{el}[Ti(a^5F_1)] = 0.81$ eV.²⁹ Consequently, for the $V(a^6D) + NO$ and O_2 systems, the model predicts crossing distances, R_x , of 2.23 and 2.38 Å and leads to values of $k_{ET} = 90 \times 10^{-12}$ and 100×10^{-12} $cm^3 s^{-1}$, respectively. While the ET model predicts that ground-state $Ti(a^3F)$ should react slower than ground-state $V(a^4F)$ with NO and O_2 , it predicts that reaction of excited-state $Ti(a^5F)$ should be faster than that of $V(a^6D)$. We have recently begun studies involving the reactions

of V(a^6D) with several neutral gases, and our preliminary results for the reaction of V($a^6D_{1/2}$) with NO and O₂ lead to effective bimolecular rate constants of $(95 \pm 30) \times 10^{-12}$ and $(83 \pm 30) \times 10^{-12} \text{ cm}^3 \text{ s}^{-1}$ for these systems,⁵⁶ in close quantitative agreement with the calculated values.

Given the assumption of a flat neutral surface, it is not surprising that the ET mechanism does a better quantitative job of predicting the rate constants for reaction of excited-state Ti(a^5F) and V(a^6D) species than for the ground-state atoms since the crossing of the ion-pair and neutral surfaces occurs at longer reagent distances. The observation that the rate constants for reaction of Ti(a^5F) with NO and O₂ are essentially identical and in quantitative agreement with the values predicted by the ET model, while the measured rate constants for reaction of Ti(a^3F) with NO and O₂ do not follow the ordering predicted by the ET model and are not in quantitative agreement, suggests that additional constraints are present along the surface evolving from the Ti(a^3F) state. RW suggested that the change in equilibrium bond length from OX to OX⁻ (which is +0.11 Å for NO and +0.13 Å for O₂) might explain the increased reactivity of NO compared with O₂ since less energy might be required to stretch NO to form NO⁻ than O₂.¹⁶ The similarity in the rate constants that we measure for Ti(a^5F) with NO and O₂ shows that such a constraint is not an important factor for the Ti(a^5F) reactions.

Our present results for the reactions of Ti(a^5F) with NO, O₂, and N₂O are consistent with both a direct mechanism that occurs along an attractive neutral surface and an ET mechanism. Both mechanisms depend on close-range interactions of the neutral reagents. For the reaction of higher excited states of Ti, this might not be the case. For example, for the NO and O₂ system, potential surfaces evolving from excited Ti states above 3.1 and 2.5 eV, respectively, would cross the Ti⁺ + OX⁻ ion-pair surface at reagent distances in excess of the HS radii, ~ 3.7 Å. Thus, for these high-lying states of Ti the long-range harpoon mechanism supersedes the close-range ET mechanism. Experiments that probe the reactivity of these high-lying states could provide more direct information about the role of the ion-pair surfaces in these systems since rate constants in excess of the HS limit cannot be explained by considering only the interaction of the neutral reagents. We are currently beginning such investigations in order to further understand O atom abstraction by transition metal atoms.⁵⁵

Summary

We have shown that the kinetic technique introduced by RW to study the reaction of ground-state transition metal atoms can also be used to study the kinetics of depletion of excited-state metal atoms. Specifically, the 300 K rate constants for the depletion of Ti(a^5F) by interactions with NO, O₂, and N₂O have been measured to be (146 ± 17) , (135 ± 29) , and $\geq 190 \times 10^{-12} \text{ cm}^3 \text{ s}^{-1}$, respectively. Quenching of Ti(a^5F) to form Ti(a^3F) by collisions with N₂ was also studied and found to proceed much more slowly, $k_q = (6.5 \pm 2.2) \times 10^{-12} \text{ cm}^3 \text{ s}^{-1}$. The Ti(a^5F) + N₂ results combined with evidence for TiO formation from other studies suggest that depletion from interaction of Ti(a^5F) with OX is most likely due to formation of TiO via reaction 1.

Comparison of the reactivity of ground-state Ti(a^3F) and excited-state Ti(a^5F) shows that the latter state reacts much more efficiently with all OX. These results are consistent with two reaction mechanisms that have been proposed for the reaction of Ti(a^3F). The first depends on the ability of neutral Ti to directly abstract an O atom and explains the inefficiency of the Ti(a^3F) reactions as a barrier that arises from a crossing between the surfaces evolving from a repulsive Ti($a^3F, 4s^2 3d^2$) state and the attractive Ti($a^3F, 4s^1 3d^3$) state. The second involves an electron-transfer process to form Ti⁺ + OX⁻ followed by transfer of O⁻ to Ti⁺. This process is similar to the harpoon mechanism.

Acknowledgment. This work is supported by grants (Nos. 92034, 03403003, and 04233217) from the Japanese Ministry of Education, Science, and Culture. D.E.C. gratefully acknowledges support from the Japan Society for the Promotion of Science for a JSPS fellowship.

References and Notes

- (1) Murad, E. *J. Geophys. Res.* **1978**, *83*, 5525. Murad, E. *Tech. Rep. AFGL-TR-77-0235*; Air Force Geophys. Lab. Hanscom Air Force Base, MA, 1977. Brown, T. L. *Chem. Rev.* **1973**, *73*, 645.
- (2) Johnsen, R.; Castell, F. R.; Biondi, M. A. *J. Chem. Phys.* **1974**, *61*, 5404.
- (3) Fisher, E. R.; Elkind, J. L.; Clemmer, D. E.; Georgiadis, R.; Loh, S. K.; Aristov, N.; Sunderlin, L. S.; Armentrout, P. B. *J. Chem. Phys.* **1990**, *90*, 2676.
- (4) Rutherford, J. A.; Vroom, D. A. *J. Chem. Phys.* **1976**, *65*, 4445.
- (5) Kappes, M. M.; Staley, R. H. *J. Phys. Chem.* **1981**, *85*, 942.
- (6) Ferguson, E. E.; Fehsenfeld, F. C. *J. Geophys. Res., Space Physics* **1968**, *73*, 6215.
- (7) Dheandhanoo, S.; Chatterjee, B. K.; Johnsen, R. *J. Chem. Phys.* **1985**, *83*, 3327.
- (8) Armentrout, P. B.; Beauchamp, J. L. *Chem. Phys.* **1980**, *50*, 27.
- (9) Armentrout, P. B.; Halle, L. F.; Beauchamp, J. L. *J. Chem. Phys.* **1982**, *76*, 2449.
- (10) Clemmer, D. E.; Elkind, J. L.; Aristov, N.; Armentrout, P. B. *J. Chem. Phys.* **1991**, *95*, 3387.
- (11) Rowe, B. R.; Fahey, D. W.; Ferguson, E. E.; Fehsenfeld, F. C. *J. Chem. Phys.* **1981**, *75*, 3325.
- (12) Clemmer, D. E.; Dalleska, N. F.; Armentrout, P. B. *J. Chem. Phys.* **1991**, *95*, 7263.
- (13) Clemmer, D. E.; Dalleska, N. F.; Armentrout, P. B. *Chem. Phys. Lett.* **1992**, *190*, 259.
- (14) Clemmer, D. E., Ph.D. Thesis, University of Utah, 1992.
- (15) Ritter, D.; Weisshaar, J. C. *J. Phys. Chem.* **1989**, *93*, 1576.
- (16) Ritter, D.; Weisshaar, J. C. *J. Phys. Chem.* **1990**, *94*, 4907.
- (17) Mitchell, S. A.; Hackett, P. A. *J. Chem. Phys.* **1990**, *93*, 7822.
- (18) Parnis, M. J.; Mitchell, S. A.; Hackett, P. A. *J. Phys. Chem.* **1990**, *94*, 8152.
- (19) Futerko, P. B.; Fontijn, A. *J. Chem. Phys.* **1993**, *98*, 7004.
- (20) Futerko, P. B.; Fontijn, A. *J. Chem. Phys.* **1991**, *95*, 8065.
- (21) Dubois, L. H.; Gole, J. L. *J. Chem. Phys.* **1977**, *66*, 779.
- (22) Gole, J. L.; Preuss, D. R. *J. Chem. Phys.* **1977**, *66*, 3000.
- (23) Chalek, C. L.; Gole, J. L. *Chem. Phys.* **1977**, *19*, 59.
- (24) Manos, D. M.; Parson, J. M. *J. Chem. Phys.* **1975**, *63*, 3575.
- (25) Parson, J. M.; Geiger, L. C.; Conway, T. J. *J. Chem. Phys.* **1981**, *74*, 5595.
- (26) Raiche, G. A.; Belbruno, J. J. *Chem. Phys. Lett.* **1987**, *134*, 341.
- (27) Felder, W.; Fontijn, A. *Chem. Phys. Lett.* **1975**, *34*, 398. Weisenfeld, J. R.; Yuen, M. J. *Chem. Phys. Lett.* **1976**, *42*, 293.
- (28) Armentrout, P. B. Electronic State Specific Transition Metal Ion Chemistry. *Annu. Rev. Phys. Chem.* **1990**, *41*, 313.
- (29) Sugar, J.; Corliss, C. *J. Phys. Chem. Ref. Data* **1985**, *14*, Suppl. No. 2.
- (30) Jonah, C. D.; Zare, R. N.; Ottinger, Ch. *J. Chem. Phys.* **1972**, *56*, 263.
- (31) Kolb, C. E.; Elgin, J. B. *Nature* **1976**, *263*, 488.
- (32) Garstang, R. H. *Mon. Not. R. Astron. Soc.* **1962**, *124*, 321.
- (33) The measured lifetime for the parity-forbidden transition of the Mn⁺(a^5S) first excited state is 5.8 ± 0.7 s. See: Strobel, F.; Ridge, D. P. *J. Phys. Chem.* **1989**, *93*, 3635.
- (34) Ho, J.; Ervin, K. M.; Lineberger, W. C. *J. Chem. Phys.* **1990**, *93*, 6987.
- (35) Schultz, R. H.; Armentrout, P. B. *Int. J. Mass Spectrom. Ion Processes* **1991**, *95*, 121.
- (36) To produce Ti*, green light (532 nm) from a Nd:YAG laser was focused through the source window onto the end of a Ti target rod. The end of the Ti rod was cut at a 45° angle relative to the flow direction so that vaporized atoms were emitted into the center of the flow rather than restricting them to the vaporized side.
- (37) The TiO was formed in the reaction region of RW's instrument.
- (38) Ager, J. W.; Talcott, C. L.; Howard, C. J. *J. Chem. Phys.* **1986**, *85*, 5584.
- (39) Imamura, T.; Imajo, T.; Suzuki, S.; Koyano, I. *J. Chem. Phys.* **1993**, *98*, 6248.
- (40) Imajo, T.; Imamura, T.; Koyano, I. *Chem. Phys. Lett.* **1990**, *160*, 143.
- (41) Imamura, T.; Imajo, T.; Koyano, I. *Chem. Phys. Lett.* **1991**, *178*, 399.
- (42) Albritton, D. L. *At. Data Nucl. Data Tables* **1978**, *22*, 1.
- (43) Although it seems most reasonable that the increase observed in the Ti + N₂O system is quenching via process 6, we cannot rule out the possibility that other chemical species contribute. For example, a small population of Ti₂ in the beam could react with N₂O to form Ti(a^5F) and TiO. Spectroscopic (Doverstal, M.; Lindgren, B.; Sassenberg, U.; Arrington, C. A.; Morse, M. D. *J. Chem. Phys.* **1992**, *97*, 7087) and theoretical (Bauschlicher, C. W., Jr.; Partridge, H.; Langhoff, S. R.; Rosi, M. *J. Chem. Phys.* **1991**, *95*, 1057) studies of Ti₂ have noted that diabatic dissociation of several of the low-lying

states of Ti_2 leads to formation of $Ti(a^3F) + Ti(a^5F)$. It seems unlikely that N_2O favors this process while O_2 and NO do not, however.

(44) The hard-sphere rate constant is calculated by $k_{HS} = \pi/4(d_M + d_{OX})^2 \langle v \rangle$. The diameters of the NO , O_2 , N_2O , and N_2 molecules are 3.47, 3.43, 3.88, and 3.68 Å as given in Hirschfelder, J. O.; Curtis, C. F.; Bird, R. B. *Molecular Theory of Gases and Liquids*; Wiley: New York, 1954; Table I-A. The diameter of Ti is taken to be 4.00 Å (Fischer, C. F. *The Hartree-Fock Method for Atoms*; Wiley: New York, 1977 as cited in ref 16). All Ti states are assumed to have the same diameter. The mean relative velocity, $(8kT_B/\pi\mu)^{1/2}$, was used for $\langle v \rangle$ where k_B , T , and μ were the Boltzmann's constant, temperature, and reduced mass, respectively.

(45) The HS model gives an upper limit for k_6 for Ti^* states below 3.37 eV. For higher states, the electron-transfer model predicts larger values of k_6 , but the radiative lifetimes of these states should be short since many transitions are allowed. Thus, it is likely that process 6 involves states below 3.37 eV and that the HS model is a valid limit for k_6 .

(46) One way to estimate the relative concentration of $Ti(a^3F)$ and $Ti(a^5F)$ is to compare the relative LIF intensities. However, the LIF intensities are so different that they cannot be measured at same sensitivity of the PMT. The LIF lines of $Ti(a^3F)$ were measured by 400 V of the high voltage, while the LIF lines of $Ti(a^5F)$ were only detected by more than 700 V. Since the difference in sensitivities between these two high voltages is estimated to be 50, the concentration of $Ti(a^5F)$ must be less than 1/50 of $Ti(a^3F)$.

(47) Thermochemistry derived from values of $\Delta H_f^\circ_{298}$ given in Chase, M. W.; Davies, C. A.; Downey, J. R.; Frurip, D. J.; McDonald, R. A.; Syverud, A. N. *J. Phys. Chem. Ref. Data* 1985, 14, Suppl. 1 (JANAF tables).

(48) $D^\circ_{298}(TiN) = 114 \pm 8$ kcal/mol as taken from Stearns, C. A.; Kohl, F. J. *High Temp. Sci.* 1970, 2, 146.

(49) Clemmer, D. E.; Honma, K., unpublished results.

(50) In this case, the term *correlate* refers to preservation of the electron configuration and the total electronic state symmetry.

(51) Huber, K. P.; Herzberg, G. *Constants of Diatomic Molecules*; Van Nostrand-Reinhold: New York, 1979.

(52) Merer, A. J. *Annu. Rev. Phys. Chem.* 1989, 40, 407.

(53) Levine, R. D.; Bernstein, R. B. *Molecular Reaction Dynamics and Chemical Reactivity*; Oxford University Press: New York, 1987.

(54) The electron affinities of NO and O_2 are 0.024, and 0.440 eV as taken from Drzaic, P. S.; Marks, J.; Brauman, J. I. In *Gas Phase Ion Chemistry*; Bowers, M. T., Ed.; Academic Press: New York, 1984; Vol. 3. The vertical electron affinity of N_2O is -0.2 eV as given in Lias, S. G.; Bartmess, J. E.; Leibman, J. F.; Holmes, J. L.; Levin, R. D.; Mallard, W. G. *J. Phys. Chem. Ref. Data* 1988, 17 (Suppl. 1).

(55) We note that k_{ET} increases if a value for the adiabatic EA of N_2O is used rather than the vertical EA. Usually vertical IEs and EAs are used because the electron is transferred at long reagent distances. However, in the present system the ion-pair and neutral surfaces cross at close reagent distances, and this may allow for significant geometry changes, and hence the electron to be transferred adiabatically.

(56) Clemmer, D. E.; Honma, K., work in progress.